

# One4Many-StablePacker: An Efficient Deep Reinforcement Learning Framework for the 3D Bin Packing Problem

Lei Gao<sup>1</sup>, Shihong Huang<sup>2</sup>, Shengjie Wang<sup>2</sup>, Hong Ma<sup>2\*</sup>, Feng Zhang<sup>1</sup>, Hengda Bao<sup>1</sup>, Qichang Chen<sup>1</sup>, Weihua Zhou<sup>3</sup>

<sup>1</sup>S.F. Technology Co., Ltd., 518054, Shenzhen, China

<sup>2</sup>Polytechnic Institute, Zhejiang University, 310015, Hangzhou, China

<sup>3</sup>School of Management, Zhejiang University, 310058, Hangzhou, China

## Abstract

The three-dimensional bin packing problem (3D-BPP) is widely applied in logistics and warehousing. Existing learning-based approaches often neglect practical stability-related constraints and exhibit limitations in generalizing across diverse bin dimensions. To address these limitations, we propose a novel deep reinforcement learning framework, One4Many-StablePacker (O4M-SP). The primary advantage of O4M-SP is its ability to handle various bin dimensions in a single training process while incorporating support and weight constraints common in practice. Our training method introduces two innovative mechanisms. First, it employs a weighted reward function that integrates loading rate and a new height difference metric for packing layouts, promoting improved bin utilization through flatter packing configurations. Second, it combines clipped policy gradient optimization with a tailored policy drifting method to mitigate policy entropy collapse, encouraging exploration at critical decision nodes during packing to avoid suboptimal solutions. Extensive experiments demonstrate that O4M-SP generalizes successfully across diverse bin dimensions and significantly outperforms baseline methods. Furthermore, O4M-SP exhibits strong practical applicability by effectively addressing packing scenarios with stability constraints.

## Introduction

The three-dimensional bin packing problem (3D-BPP) is a classic combinatorial optimization problem (COP) that aims to pack a set of items with known dimensions into a bin to maximize space utilization while satisfying geometric feasibility constraints, such as non-overlapping and fully enclosed placements (Fowler, Paterson, and Tanimoto 1981). Existing approaches, including exact and heuristic algorithms (Chen, Lee, and Shen 1995; Martello, Pisinger, and Vigo 2000a; Wu et al. 2010; Crainic, Perboli, and Tadei 2009), face scalability and quality limitations for large instances (Wu et al. 2023). Recent efforts have applied deep reinforcement learning (DRL) to develop packing solutions from data or interactions, demonstrating superior empirical performance compared to heuristic rules (Zhang, Zi, and Ge 2021). However, most DRL-based studies focus solely on maximizing volume utilization, neglecting stability-related constraints critical for real-world packing, such as weight

stability (prohibiting heavy-over-light stacking) and base support (ensuring sufficient contact area) (Zhou et al. 2024). These constraints, essential for generating feasible solutions, remain underexplored in prior work (Wu et al. 2023). Moreover, most existing DRL models are trained for fixed bin sizes (see Table 1), requiring retraining when bin dimensions vary, which limits their practical deployment in logistics with diverse bin specifications (Xiong et al. 2024).

To address these limitations, we propose the One4Many-StablePacker (O4M-SP) framework. “One4Many” denotes the model’s ability to generalize across bins with varied dimensions, particularly those not encountered during training, without requiring retraining. “Stable” emphasizes the model’s explicit integration of stability-related constraints to ensure real-world feasibility. Stability constraints, along with “cross-dimension” generalization, increase problem complexity. Moreover, existing DRL methods often face challenges with single-reward functions and premature policy entropy collapse (Wang et al. 2025b). To address these challenges, we develop an efficient DRL-based framework by constructing a weighted reward function that combines loading rate with a novel height difference metric and implementing clipped policy gradient optimization with policy drifting to promote exploration at critical decision nodes.

The main contributions are summarized as follows. First, we propose O4M-SP, the first DRL framework for offline 3D-BPP that simultaneously addresses stability constraints and generalizes across diverse bin dimensions in a single training process. Second, we design a new weighted reward function to mitigate the limitations of single-reward functions, and conduct policy entropy control at critical decision nodes to promote exploration and enhance policy quality. Finally, we demonstrate that O4M-SP achieves superior packing performance over baseline methods and confirm that O4M-SP effectively enforces practical stability constraints.

## Related Work

### Deep reinforcement learning for solving COPs

Combinatorial optimization is a key research topic in operations research and computer science (Schrijver 2002), playing essential roles in path planning (Veres and Moussa 2019; Li et al. 2024, 2025), resource allocation (Huang et al. 2025), and task scheduling (Dolgui et al. 2019). Current methods

\*Corresponding author

for solving COPs include traditional algorithms, deep reinforcement learning (DRL), and hybrid approaches. Due to their NP-hard nature, exact methods ensure optimality but are computationally inefficient, while heuristics improve speed yet face limitations in large-scale, real-time scenarios. DRL has recently demonstrated advantages in solving COPs by modeling discrete optimization tasks as sequential decision-making processes (Wu et al. 2024), enabling efficient strategies to be learned through interactions between policy networks and the environment. Specifically, neural networks generate strategies trained via supervised learning (Fu, Qiu, and Zha 2021) or reinforcement learning (Bello et al. 2016). Early work focused on classic graph optimization problems. Khalil et al. (2017) integrated graph embeddings with Q-learning to achieve near-optimal solutions and strong generalization for minimum vertex cover and maximum cut problems. Later, Luo et al. (2023) introduced a Light Encoder and Heavy Decoder (LEHD) Transformer that dynamically captures node relationships, achieving effective generalization from small TSP and CVRP instances to solve large-scale problem instances with up to 1000 nodes. Regarding hybrid methods, Feng and Yang (2025) proposed the Suboptimal-demonstration-guided Reinforcement Learning (SORREL) framework, which outperforms prior learning-based methods for mixed integer linear programming problems in both branching quality and training efficiency.

### Deep reinforcement learning for solving 3D-BPP

Recent advances in DRL have demonstrated strong potential for solving 3D-BPP. In Table 1, we summarize recent learning-based approaches for solving offline 3D-BPP.

To our knowledge, Hu et al. (2017) first introduced a pointer network with policy gradient to minimize bin surface area for a novel variant of 3D-BPP, establishing the foundation for sequential decision frameworks for 3D-BPP. Subsequent efforts focused on model and algorithmic improvements. The approach in Duan et al. (2018) applied the more stable PPO algorithm, while Laterre et al. (2018) combined deep neural networks (DNNs) with Monte Carlo Tree Search (MCTS) and introduced center-of-mass support constraints. With the rise of convolutional neural networks (CNNs), height map-based state representations became prevalent (Goyal and Deng 2020; Jiang, Cao, and Zhang 2021a,b; Zhao, Li, and Lin 2024). Height maps provide a compact encoding of space occupancy and, when paired with CNNs, deliver strong performance for fixed-size bins. However, the fixed input structure of CNNs restricts their generalization to variable-sized bins, limiting practical applicability. Recent studies have aimed to address this limitation: Li et al. (2020); Zhang, Zi, and Ge (2021) leverage self-attention to model inter-item and item-bin relationships directly, demonstrating promise in handling variable-sized bins. The approach in Hu et al. (2020) combines CNNs (height maps) with attention mechanisms (for item features), introducing a stability ratio objective function and “convex hull checks”, marking an early effort to integrate spatial efficiency with stability.

Despite the importance of stability in real-world pack-

ing, our survey reveals that existing DRL-based offline 3D-BPP research has largely overlooked this aspect. As shown in Table 1, only Laterre et al. (2018) introduced center-of-mass support constraints and Hu et al. (2020) provided a simplified stability guarantee through convex hull checks. Notably, progress has been made in online 3D-BPP, where bottom support constraints have been considered and modeled (Yang et al. 2023; Zhao et al. 2021; Zhou et al. 2024). These studies offer valuable insights for incorporating complex yet practical stability constraints into offline 3D-BPP.

## Methodology

### Problem Statement and Formulation

We state 3D-BPP with stability constraints studied in this work as follows. The problem seeks a non-overlapping placement of  $N$  cuboid items into a bin. Each item  $i$  has dimensions  $(l_i, w_i, h_i)$ , where  $l_i$ ,  $w_i$ , and  $h_i$  represent its length, width, and height, respectively. Similarly, the bin has fixed dimensions  $(L, W, H)$ , where height  $H = \sum_{i=1}^N \max(l_i, w_i, h_i)$ . The objective is to maximize space utilization  $\eta$ :

$$\eta = \frac{\sum_{i=1}^N w_i l_i h_i}{WLH_N}, \quad (1)$$

$H_N$  is the minimal bin height required to enclose all items. The  $X$ ,  $Y$ , and  $Z$  axes correspond to the bin’s length, width, and height, respectively. All items must be axis-aligned, with edges parallel to the axes, and may be placed with any face as the base. Beyond these geometric constraints, we incorporate stability constraints (Figure 2(b)), comprising two main parts:

**Support Constraints:** When an item is placed in the bin and its bottom surface simultaneously contacts one or more items already in the bin, the contact area with each item below is computed, and their sum is denoted as  $F$ . The bottom area of the newly placed item is denoted as  $f$ . It is required that  $F \geq r_s f$ , where  $r_s$  is the predefined support ratio.

**Weight Constraints:** When an item  $j$  with weight  $G_j$  is placed in the bin and its bottom surface just contacts one item below. The item below is denoted as item  $i$  with weight  $G_i$ . It is required that  $G_j \leq r_w G_i$ , where  $r_w$  is the predefined weight ratio.

We formulate the above 3D-BPP as a Markov Decision Process (MDP), which is a tuple  $\langle S, A, P, R, \gamma \rangle$ .

**State:** At time step  $t$ , the environment state is defined as  $s_t = \{s_{bin}, s_{valid.items}\}$ . First, for the bin state  $s_{bin}$ , existing methods have limitations: height maps: height maps (Zhao, Li, and Lin 2024) and weighted 3D voxel grids (Yang et al. 2023), which rely on CNNs, limit the model’s ability to generalize across diverse bin dimensions; the item list representation (Zhao, Yu, and Xu 2021) not fully capture remaining space; and the Empty Maximal Space (EMS)-based PG representation (Xiong et al. 2024) captures all available space but has a rather weak representation of packed items. In this work, we propose a new state representation that combines the strengths of these approaches. At time step  $t$ , with  $n$  items packed,  $s_{bin}$  is represented as an  $(n+2) \times 7$  matrix: The first row contains the bin’s attributes. The second

Approach	Bin Size	Module	State	Reward	Stability	RL
Hu et al. (2017)	–	PN	item size	terminal (surf.)	none	PG+BS
Duan et al. (2018)	–	PN	item size	terminal (surf.)	none	PPO
Laterre et al. (2018)	–	DNN	item	terminal (surf.)	center supp.	MCTS
Goyal and Deng (2020)	Single	CNN	voxel	step. (LR)	none	PPO
Hu et al. (2020)	Single	CNN+Attn.	HM+size	terminal (util.+stab.)	conv. hull	AC
Li et al. (2020)	Multi.	Attn.	item	step. (LR)	none	AC
Jiang, Cao, and Zhang (2021a)	Single	CNN	HM+item	step. (LR)	none	A2C
Zhang, Zi, and Ge (2021)	Multi.	CNN+Attn.	item+frontier	terminal (util.)	none	PO
Jiang, Cao, and Zhang (2021b)	Single	CNN+Attn.	HM+item	step. (LR)	none	A2C
Zhao, Li, and Lin (2024)	Single	CNN+Attn.	HM+item	step. (LR)	none	SAC
Wang et al. (2025a)	Single	PN+GRU+Attn.	HM+item	step. (LR+comp.+pyr.)	none	AC
<b>Our Work</b>	<b>Multi.</b>	<b>Attention</b>	<b>Bin+item</b>	<b>step. (LR+HD)</b>	<b>supp.+weight</b>	<b>PPO+Entropy</b>

Table 1: Comparison of DRL-based approaches for the offline 3D-BPP. Abbreviation: Point Network (PN), Policy Gradient (PG), Beam Search (BS), Proximal Policy Optimization (PPO), Deep Neural Network (DNN), Monte Carlo Tree Search (MCTS), Convolutional Neural Networks (CNN), Actor-Critic (AC), Advantage Actor-Critic (A2C), Prioritized Oversampling (PO), Soft Actor-Critic (SAC), Gated Recurrent Unit (GRU), Attention (Attn.), Height Map (HM), Surface (Surf.), Stepwise (Step.), Utilization (Util.), Loading Rate (LR), Support (Supp.), Compactness (Comp.), Pyramid (Pyr.), Height Difference (HD)

row contains the attributes of the current space. The subsequent  $n$  rows represent the attributes of the packed items. A right-handed coordinate system is used with the front-left-bottom (FLB) vertex of the bin as the origin; columns 1–3 of the matrix represent the FLB coordinates, with the bin’s coordinates being  $(0, 0, 0)$ , columns 4–6 represent the length, width, and height, and column 7 represents the weight, with the weights of the bin and the current space being 0. The current space (highlighted in orange in Figure 2(a)) is selected from all available spaces (highlighted in blue  $S_1$  to  $S_5$  in Figure 2(a)) generated by the Empty Maximal Space (EMS) method using a screening heuristic. The screening heuristic is as follows: The loading sequence follows an XYZ order (prioritizing the X-axis, then the Y-axis, and finally the Z-axis) to maximize floor and space utilization. In our implementation, all available spaces are pushed onto a stack. The stability of the top space on the stack is evaluated, and if stable, it is selected as the current space. If unstable, the top space is popped from the stack, and the next top is evaluated.

Second, the representation of the valid items state  $s_{valid\_items}$  is closely tied to the stability check. At time step  $t$ , if no available space exists, no valid item or valid action is available. Otherwise, the stack containing available spaces is checked as follows: the top space is evaluated, and the remaining items and their rotations are examined to identify valid orientations that can be placed in the space. If no valid orientations exist, the top space is popped from the stack, and the next top space is evaluated; if valid orientations are found, a stability check is performed on the candidate actions. Actions that pass the stability check are included in  $s_{valid\_items}$ , and the top space in the stack is selected as the current space. At time step  $t$ , with  $k$  types of valid items, the state  $s_{valid\_items}$  is represented as a  $k \times 5$  matrix: columns 1–3 represent the length, width, and height of each item, column 4 represents the remaining quantity of each item, and column 5 represents the weight of each item.

**Action:** Given the state  $s_t$  at time step  $t$ , the action  $a_t$  selects a valid item, determines its rotation, and places it at the

front-left-bottom (FLB) corner of the current space. The dimension of the action space depends on the number of valid items and their feasible rotations.

**State Transition:** State transitions are deterministic. Specifically, given the state  $s_t$ , action  $a_t$  is sampled according to the policy  $\pi(\cdot|s_t)$ , transitioning deterministically to the state  $s_{t+1}$ .

**Reward:** An effective stepwise reward provides meaningful intermediate signals to guide policy exploration. Existing methods employ mainly a single reward, such as volume change (Li et al. 2022), volume gap reduction (Li et al. 2020), loading-rate change (Zhang and Shuai 2024), or gap-ratio reduction (Zhao, Li, and Lin 2024), which may lead policies to converge prematurely to local optima. In this work, we introduce a new weighted reward function:

$$r_t = \alpha_1 r_t^{LR} + \alpha_2 r_t^{HD} \quad (2)$$

where  $r_t^{LR}$  denotes the loading rate reward (Eq. 3),  $r_t^{HD}$  denotes the height difference reward for the packing layout (Eq. 4), and  $\alpha_1, \alpha_2$  are hyperparameters.

$$r_t^{LR} = \frac{\sum_{i=1}^t w_i l_i h_i}{WLH_t} - \frac{\sum_{i=1}^{t-1} w_i l_i h_i}{WLH_{t-1}} \quad (3)$$

$$r_t^{HD} = (H_t - H_t') - (H_{t-1} - H_{t-1}') \quad (4)$$

In Equations (3)–(4),  $H_t$  denotes the maximum height of all packed items at step  $t$ , and  $H_t'$  denote the second maximum height of all packed items. We normalize the difference between  $H_t$  and  $H_t'$ , assigning larger rewards to smaller height difference metrics to encourage flatter packing.

Figure 1 illustrates the effect of the proposed weighted reward function compared with the loading-rate-only reward function. For example, at Step 1, the loading-rate-only reward function helps select the largest item (rotated to minimize height), which unfortunately blocks subsequent placement of large items in the first packing layer. In contrast, the weighted reward function helps select a smaller item,

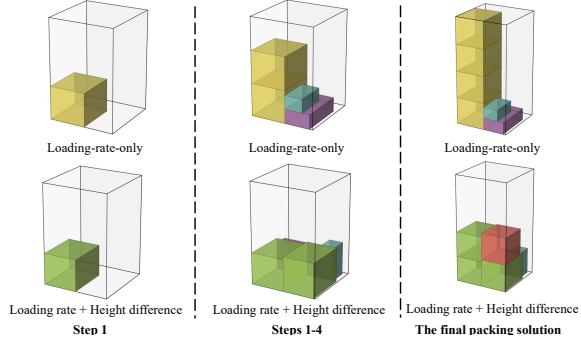


Figure 1: Space selection with different reward functions

slightly reducing the loading rate while improving the flatness of the packing layer. Figure 1 shows that the loading-rate-only reward aggressively promotes vertical stacking, whereas the weighted reward achieves significantly higher overall utilization by the end. Moreover, when multiple actions yield identical improvements in the overall loading rate, the weighted reward would prioritize actions that produce smaller height differences, preserving space for subsequent decisions. The height difference reward effectively converts potential future gains from flatness into immediate rewards, addressing the limitations of single-reward approaches.

## Network Architecture

The network architecture significantly influences the learning and generalization capabilities of DRL algorithms. To address limitations of existing approaches, we propose a novel state representation that enables model generalization across bins of varied dimensions and introduce a stability checker module to ensure adherence to physical stability constraints. The model adopts an actor-critic framework, as shown in Figure 2. The packing environment provides the bin state, valid item candidates, and rotation information, which are encoded into 256-dimensional embeddings. These embeddings are processed by the feature extractor, actor, and critic networks to produce action probabilities and value estimates, respectively. The network architecture comprises the following core components:

**Feature Extractor:** The feature extractor consists of eight identical encoder blocks, each comprising a self-attention layer, a cross-attention layer, and a feed-forward network (FFN), followed by residual connections and layer normalization. The self-attention layer integrates information from the bin, current space, and placed items to produce an updated state vector  $S_{new}$ . Along with  $S_{valid.items}$ , it is fed into and processed by the cross-attention layer to enable inter-feature interactions. The FFN in each block performs nonlinear transformations on the attention outputs, enhancing feature expressiveness.

**Actor and Critic Networks:** Both are two-layer multi-layer perceptrons (MLPs) with GELU activation functions. The actor network processes state and rotation features separately, then combines them multiplicatively to produce a

probability distribution over actions. The critic network directly estimates the state value from the packing state features.

## Training Method

A core challenge in training DRL neural networks lies in the exploration-exploitation trade-off (Sutton 1988). Policy entropy, an indicator of exploration capability reflecting action diversity, typically decreases as model performance improves (Cui et al. 2025). Traditional PPO employs entropy regularization; however, these global entropy-loss methods lack precision, leading to premature policy entropy collapse and suboptimal local solutions early in training. To address this, we propose a tailored entropy-control scheme integrated into PPO for 3D-BPP.

First, we note that prior studies identify critical decision nodes where policy entropy decreases significantly, narrowing the action space (Wang et al. 2025b). Accordingly, we selectively apply entropy control at critical decision nodes during packing to restrict high-confidence decisions and enhance the model’s ability to escape local optima. We observe that in 3D-BPP, entropy consumption is most pronounced during the initial steps, with entropy curves for varying item quantities shown in Figure 3. Early placement decisions significantly shape the remaining space in the bin, and suboptimal early actions (e.g., occupying critical positions or creating fragmented spaces) have irreversible impacts, highlighting the critical role of initial steps during packing.

Next, as indicated by Cui et al. (2025), when policy parameters are updated from  $\theta^k$  to  $\theta^{k+1}$ , the change in policy entropy  $H$  for a given state  $s$  follows the pattern presented in Equation (5).

$$\Delta H \approx -\beta \text{Cov}_{a \sim \pi_\theta^k(\cdot|s)}(\log \pi_\theta^k(a|s), A(s, a)) \quad (5)$$

where  $\Delta H = H(\pi_\theta^{k+1}|s) - H(\pi_\theta^k|s)$  and  $H(\pi_\theta^k|s) = -\sum_a \pi_\theta^k(a|s) \log \pi_\theta^k(a|s)$  represents the policy entropy at step  $k$  for state  $s$ ,  $A(s, a)$  denotes the advantage of action  $a$ , and  $\text{Cov}_{a \sim \pi_\theta^k(\cdot|s)}(\cdot, \cdot)$  denotes the covariance calculated for all possible actions  $a$  under the policy  $\pi_\theta^k(\cdot|s)$  at step  $k$ . It reveals that when the covariance at step  $k$  is high, forward exploration leads to significant policy entropy loss, implying that high-covariance nodes are critical decision nodes.

Based on these findings, we conduct policy entropy control on the above two types of critical decision nodes. For nodes  $N_{high.cov}$  with high covariance, we extract a small portion  $\phi \cdot N_{high.cov}$  and apply the clipped policy gradient optimization proposed in (Cui et al. 2025):

$$p_t(\theta) = \begin{cases} \frac{\pi_\theta(a_t|s_t)}{\pi_{\theta_{old}}(a_t|s_t)}, & t \notin \phi N_{high.cov} \\ 0, & t \in \phi N_{high.cov} \end{cases} \quad (6)$$

This approach enables the model to explore high-covariance nodes while restricting certain nodes to perform only forward propagation, effectively mitigating the neural network’s overfitting and preserving policy entropy. However, for the nodes  $N_{first.step}$  corresponding to initial item placements, clipping may adversely affect the model’s

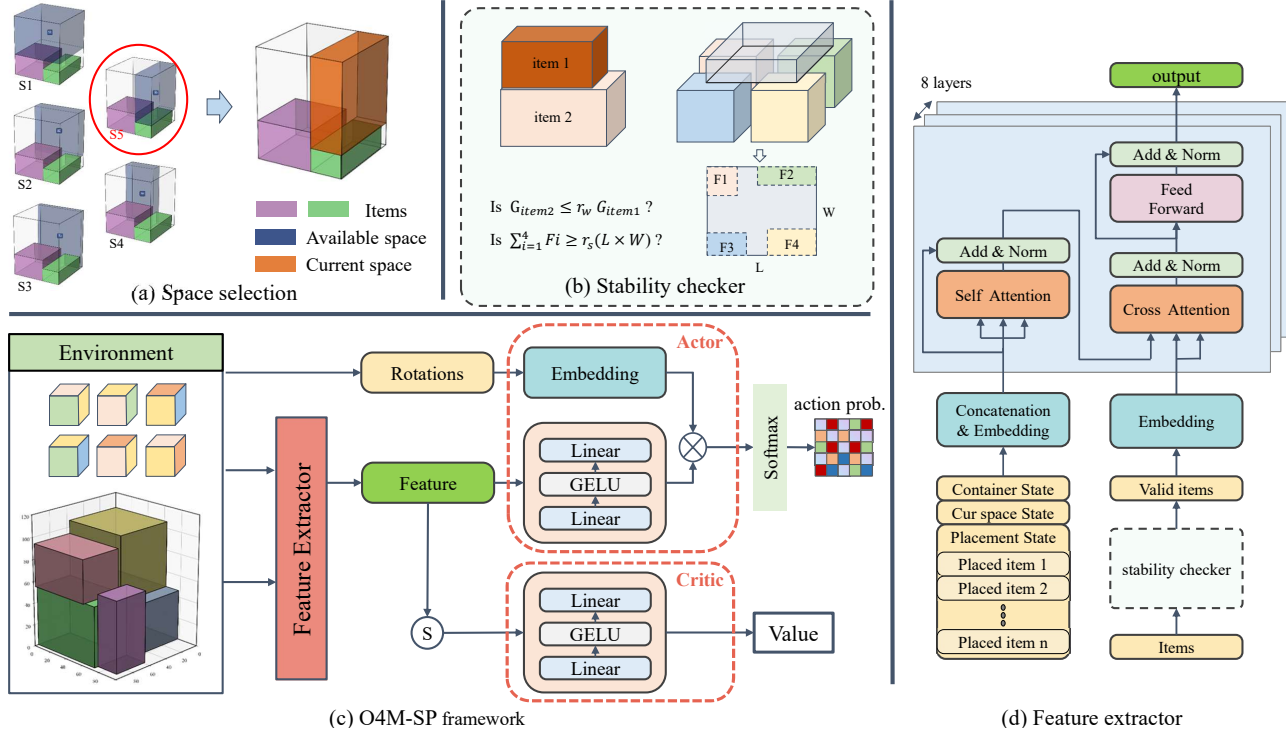


Figure 2: Overview of our method. (a) Space selection: A heuristic for selecting the space for placement. (b) Stability checker: Enforces support and weight constraints. (c) O4M-SP framework: Extracts features from environmental information and uses actor and critic networks to generate action probabilities and value estimates. (d) Feature extractor: Eight identical encoder blocks, each comprising self-attention, cross-attention, feed-forward layers, residual connections, and layer normalization.

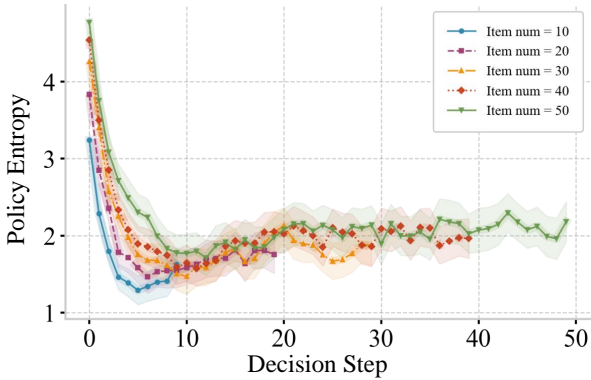


Figure 3: Variation of policy entropy with decision steps

convergence. Hence, we apply a tailored policy drifting method, similar to Liu et al. (2025).

$$J_t(\theta) = \begin{cases} J_t(\theta) & t \notin N_{first\_step} \\ J_t(\theta) - \beta P_{policy} & t \in N_{first\_step} \end{cases} \quad (7)$$

$J_p(\theta)$  denotes the policy loss term, which includes a penalty  $P_{policy} = |\log(\frac{\pi_{\theta}(a_t|s_t)}{\pi_{\theta_{old}}(a_t|s_t)})|$ . The method miti-

gates policy deviation during initial item placement, weakens backpropagation intensity, and avoids premature convergence to local optima, thereby slowing policy entropy loss.

## Experiments

### Experimental setup

We implement O4M-SP on an Ubuntu 24.04 Linux server equipped with dual AMD EPYC 9554 64-Core Processors, 768GB memory, and an NVIDIA L40S GPU with 48GB memory. Model training takes about 37 hours. The training parameters are configured as follows. Training consists of 10,000 iterations, using the Adam with Weight Decay (AdamW) optimizer (Loshchilov and Hutter 2017) with a batch size of 256. The learning rate schedule employs a warm-up phase (20 epochs) followed by cosine annealing, with an initial learning rate of  $10^{-4}$  and a minimum learning rate of  $10^{-6}$ . Performance is evaluated every 20 iterations on an independent validation set of 10,000 samples, and the best model is saved. Training incorporates an early stopping mechanism with a patience value of 100 evaluations.

### Dataset

In dataset construction, bin dimensions—length ( $L$ ), width ( $W$ ), and height ( $H$ )—are randomly generated from the interval  $[100, 450]$  following a uniform distribution, satisfying  $L \geq W \geq H$ . Item dimensions—length ( $l$ ) and width ( $w$ )—

are also uniformly generated from  $[0.05L, 0.4L]$ , with height  $h$  satisfying  $h \geq 0.1l$  (where  $l$  is the item length) to avoid extremely flat items. The dimensions and quantities of items of different types are generated as follows: First, an item type with random dimensions (length, width, and height) is created. Its quantity is generated from  $[1, 10]$  based on a given weight. The process is repeated until the total volume of the generated items exceeds the bin volume by a factor of  $r_{volume}$ , where  $r_{volume} \in [0.8, 1.2]$ .

To ensure problem feasibility, the bin height  $H$  is set to the sum of the maximum dimensions (length, width, or height) of each item. This method ensures that each instance in the training set has unique bin dimensions, item quantities, and item combinations, effectively simulating real-world instances and enhancing the model's generalization ability to solve datasets with bin dimensions not encountered during training. The validation and test sets are generated using the same method.

## Performance evaluation

To evaluate O4M-SP, we select representative, publicly available algorithms from the literature as baselines. Table 2 reports the average loading rates and their variances for 10,000 test instances after 10,000 training iterations. All experiments are conducted with a fixed bin size of  $100 \times 100 \times H$ , evaluating each method's performance on instances with 10, 16, 20, and 30 items. To investigate the effect of training sets with varied bin dimensions, we train O4M-SP on two datasets: one with fixed bin size ( $100 \times 100 \times H$ ), denoted O4M-SP(S), and another with bin dimensions independently drawn from a uniform distribution over the interval  $[100, 450]$ , denoted O4M-SP(M). Following Zhao, Li, and Lin (2024), all DRL-based methods, including ours, decode 128 samples per instance and retain the best solution.

Experimental results demonstrate that O4M-SP consistently outperforms all baseline methods across varied problem instances. Notably, O4M-SP(S) and O4M-SP(M) exhibit distinct strengths depending on instance complexity. On smaller instances (10 and 16 items), O4M-SP(M) significantly outperforms both baseline methods and O4M-SP(S), indicating that small-scale packing problems are less sensitive to bin dimensions. Training with random dimensions enhances the model's generalization ability, mitigating overfitting to fixed bin sizes. Conversely, O4M-SP(S) achieves superior performance on larger instances (20 and 30 items), suggesting that sensitivity to bin dimensions increases with problem scale. Hence, specialized training on fixed bin sizes performs better on larger problems.

## Generalization

To evaluate O4M-SP's generalization ability, we conduct two additional experiments. First, we test varied item quantities. Similar to the data generation method in Zhao, Li, and Lin (2024), where the bin size is fixed at  $100 \times 100 \times H$  with 10 items per instance, we construct the training set and test it on benchmark sets with varied sizes (10, 16, 20, and 30 items). As shown in Table 3, the model trained on the training set with 10 items generalizes well. Compared to the models in (Zhao, Li, and Lin 2024) trained on test sets with

10, 16, 20, and 30 items, O4M-SP improves loading rates by 2.41%, 0.90%, and 0.88% on the 10-, 16-, and 30-item test sets, respectively. O4M-SP performs slightly worse (1.09%) on the 20-item test set.

Second, we test on varied bin dimensions. The training and validation sets and four test sets are generated as follows. Three fixed-size test sets (B1\_30, B2\_30, B3\_30; each with 100 instances and 30 items per instance) use bins with dimensions  $(150, 230, 180)$ ,  $(176, 153, 203)$ , and  $(298, 103, 159)$ , respectively. One mixed test set (BM\_M) contains 100 instances with randomly generated bin dimensions and item quantities. Since existing learning-based methods do not generalize well to new item sizes without retraining, we compare O4M-SP against two heuristic algorithms: a widely used greedy packing algorithm (pseudo-code in the Appendix) and MCTS (Kocsis and Szepesvári 2006). As shown in Table 4, O4M-SP remains effective on test sets with varied and unseen bin dimensions, outperforming the greedy packing algorithm by 8.69% in the average loading rate. Although O4M-SP's loading rate is 5.18% lower than that of MCTS, it demonstrates significant computational efficiency, solving all instances in just a few minutes, whereas MCTS requires nearly an hour.

## Ablation study

To assess the contributions of key components in O4M-SP, namely the weighted reward (WR) and entropy control (EC), we conduct ablation studies using three variants: O4M-SP, O4M-SP without EC, and O4M-SP without WR. A multi-dimensional test dataset is constructed, comprising bins with fixed dimensions (S1:  $100 \times 100 \times H$ ; S2:  $300 \times 200 \times H$ ) and bins with dimensions randomly drawn from a uniform distribution over  $[100, 450]$ . Bin height  $H$  is set to the sum of the maximum dimensions (length, width, or height) of each items. Item quantities are either fixed (suffix \_10, \_30) or randomly generated (suffix \_M). This yields seven test sets: S1\_10, S1\_30, S2\_10, S2\_30, M\_10, M\_30, and M\_M. The ablation study results are summarized in Table 5. The policy entropy curves for each model during training are presented in Figure 4.

As presented in Table 5, across all seven test sets, the O4M-SP model significantly outperforms O4M-SP w/o EC and O4M-SP w/o WR, with average loading rates increasing by 3.37% and 1.91%, respectively. These results validate the effectiveness of WR and EC. Specifically, the WR mechanism promotes flatter packing layouts and significantly reduces wasted space, thereby exerting a more pronounced effect on the loading rates in instances with fewer items (e.g., 10 items). In contrast, the EC mechanism contributes more significantly to the loading rate in larger-scale instances (e.g., 30 items) than in smaller ones. This indicates that as the action space expands, maintaining higher policy entropy facilitates exploration of the globally optimal solutions. Training curves in Figure 4 further support these findings. Entropy curves reveal that models with EC successfully maintain high entropy levels.

	<b>GA</b>	<b>MTSL</b>	<b>CQL</b>	<b>MM</b>	<b>A2P</b>	<b>DMRL</b>	<b>O4M-SP(S)</b>	<b>O4M-SP(M)</b>
10	72.80%	49.80%	72.60%	-	-	73.00%	73.41% $\pm$ 0.0022	<b>76.12% <math>\pm</math> 0.0017</b>
16	68.50%	54.70%	69.40%	-	-	77.20%	79.14% $\pm$ 0.0011	<b>79.76% <math>\pm</math> 0.0011</b>
20	66.10%	57.30%	67.60%	71.80%	76.70%	78.90%	<b>81.44% <math>\pm</math> 0.0009</b>	80.40% $\pm$ 0.0007
30	62.60%	59.40%	69.80%	75.50%	79.70%	81.10%	<b>84.61% <math>\pm</math> 0.0005</b>	77.71% $\pm$ 0.0012

Table 2: Results: O4M-SP vs. Baseline methods, including: (1) Genetic Algorithm (GA) (Wu et al. 2010), (2) Multi-Task Selected Learning (MTSL) (Duan et al. 2018), (3) Conditional Query Learning (CQL) (Li et al. 2020), (4) Multimodal Deep Reinforcement Learning (MM) (Jiang, Cao, and Zhang 2021b), (5) Attend2Pack (A2P) (Zhang, Zi, and Ge 2021) and (6) Dynamic Multi-modal Deep Reinforcement Learning (DMRL) (Zhao, Li, and Lin 2024)

Model	10	16	20	30
DMRL-BPP	73.00%	77.20%	<b>78.90%</b>	81.10%
O4M-SP (train_10)	<b>75.41%</b>	<b>78.10%</b>	77.81%	<b>81.98%</b>

Table 3: Results: O4M-SP (train\_10) vs. Baseline methods

Model	B1_30	B2_30	B3_30	BM_M
Greedy	69.62%	68.81%	69.89%	67.38%
MCTS	84.34%	82.14%	85.73%	78.99%
O4M-SP	78.72%	77.91%	78.70%	75.13%

Table 4: Results: O4M-SP vs. Heuristic algorithms

Model	<b>S1_10</b>	<b>S1_30</b>	<b>S2_10</b>	<b>S2_30</b>	<b>M_10</b>	<b>M_30</b>	<b>M_M</b>
O4M-SP	<b>61.22</b>	<b>74.21</b>	<b>63.77</b>	<b>74.11</b>	<b>62.96</b>	<b>74.48</b>	<b>74.37</b>
O4M-SP w/o EC	58.00	69.34	60.30	70.52	59.61	71.00	72.77
O4M-SP w/o WR	58.11	72.34	61.20	72.51	60.40	73.40	73.80

Table 5: Results (%) of ablation study on multiple data sets

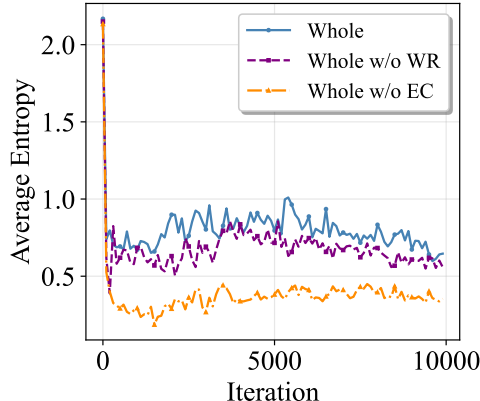


Figure 4: Policy entropy curves

### Handling Stability Constraints

To verify O4M-SP’s ability to handle practical constraints, we conduct a case study with seven item types (see Figure 5). The bin has a fixed length and width of 100, with its height set to the maximum item height multiplied by the number of items. Four scenarios are tested, where sup-

port constraints require a support ratio  $\geq 66\%$  (i.e.,  $r_s = 0.66$ ), and the weight constraints prohibit item  $A$  from being stacked solely on item  $B$  if the weight of item  $A$  is at least three times that of item  $B$  (i.e.,  $r_w = 3.0$ ). As shown in Figure 5, Scenario 1 considers neither support nor weight constraints, yielding a loading rate of 84.24%. Scenario 2 considers only support constraints, yielding a loading rate of 82.49%. Scenario 3 considers only weight constraints, yielding a loading rate of 83.37%. Scenario 4 considers both constraints, yielding a loading rate of 79.18%. From Figure 5, we observe that in Scenarios 1 and 2, the heaviest yellow item is stacked on the blue item, whereas in Scenarios 3 and 4, which consider weight constraints, the yellow item is positioned at the bottom and does not stack on other items. Scenarios 2 and 4, which consider support constraints, achieve support ratios  $\geq 66\%$ , while scenarios 1 and 3 only achieve support ratios 46% and 56%, respectively. The results reveal O4M-SP’s effectiveness in handling stability constraints and its strong potential for industrial applications.

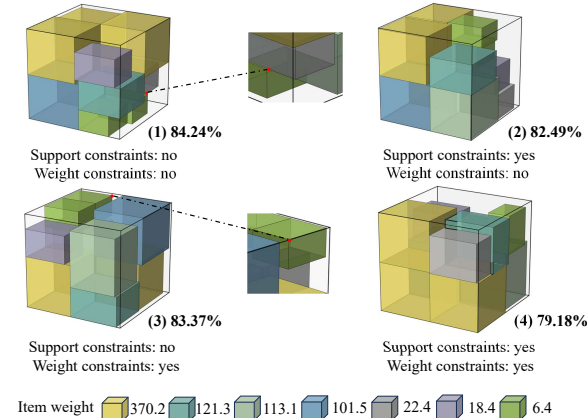


Figure 5: Visualizations for handling stability constraints

### Conclusion

We contribute a novel deep reinforcement learning framework, One4Many-StablePacker (O4M-SP), which integrates complex yet practical stability constraints to enhance real-world applicability. Its primary advantage is its “train once, apply broadly” capability, which enables generalization across diverse bin dimensions without retraining. Extensive experiments prove O4M-SP’s superiority over existing

methods across various problem instances. Future research could extend the framework to address more complex scenarios, such as irregularly shaped items and weight constraints for items contacting multiple supporting items below, thus enabling more comprehensive applications.

## References

Bello, I.; Pham, H.; Le, Q. V.; Norouzi, M.; and Bengio, S. 2016. Neural combinatorial optimization with reinforcement learning. *arXiv preprint arXiv:1611.09940*.

Chen, C.-S.; Lee, S.-M.; and Shen, Q. 1995. An analytical model for the container loading problem. *European Journal of operational research*, 80(1): 68–76.

Crainic, T. G.; Perboli, G.; and Tadei, R. 2008. Extreme point-based heuristics for three-dimensional bin packing. *Informs Journal on computing*, 20(3): 368–384.

Crainic, T. G.; Perboli, G.; and Tadei, R. 2009. TS2PACK: A two-level tabu search for the three-dimensional bin packing problem. *European Journal of Operational Research*, 195(3): 744–760.

Cui, G.; Zhang, Y.; Chen, J.; Yuan, L.; Wang, Z.; Zuo, Y.; Li, H.; Fan, Y.; Chen, H.; Chen, W.; et al. 2025. The entropy mechanism of reinforcement learning for reasoning language models. *arXiv preprint arXiv:2505.22617*.

Dolgui, A.; Ivanov, D.; Sethi, S. P.; and Sokolov, B. 2019. Scheduling in production, supply chain and Industry 4.0 systems by optimal control: fundamentals, state-of-the-art and applications. *International journal of production research*, 57(2): 411–432.

Duan, L.; Hu, H.; Qian, Y.; Gong, Y.; Zhang, X.; Xu, Y.; and Wei, J. 2018. A multi-task selected learning approach for solving 3D flexible bin packing problem. *arXiv preprint arXiv:1804.06896*.

Feng, S.; and Yang, Y. 2025. Sorrel: Suboptimal-demonstration-guided reinforcement learning for learning to branch. In *Proceedings of the AAAI Conference on Artificial Intelligence*, volume 39, 11212–11220.

Fowler, R. J.; Paterson, M. S.; and Tanimoto, S. L. 1981. Optimal packing and covering in the plane are NP-complete. *Information processing letters*, 12(3): 133–137.

Fu, Z.-H.; Qiu, K.-B.; and Zha, H. 2021. Generalize a small pre-trained model to arbitrarily large tsp instances. In *Proceedings of the AAAI conference on artificial intelligence*, volume 35, 7474–7482.

Goyal, A.; and Deng, J. 2020. Packit: A virtual environment for geometric planning. In *International Conference on Machine Learning*, 3700–3710. PMLR.

Hu, H.; Zhang, X.; Yan, X.; Wang, L.; and Xu, Y. 2017. Solving a new 3d bin packing problem with deep reinforcement learning method. *arXiv preprint arXiv:1708.05930*.

Hu, R.; Xu, J.; Chen, B.; Gong, M.; Zhang, H.; and Huang, H. 2020. TAP-Net: transport-and-pack using reinforcement learning. *ACM Transactions on Graphics (TOG)*, 39(6): 1–15.

Huang, S.; Zhu, H.; Wang, H.; Liu, K.; Liu, X.; and Zhang, Z.-H. 2025. Balancing the Trade-off between Efficiency and Equity in a Stochastic Emergency Supplies Allocation Problem. *Applied Mathematical Modelling*, 116242.

Jiang, Y.; Cao, Z.; and Zhang, J. 2021a. Learning to solve 3-D bin packing problem via deep reinforcement learning and constraint programming. *IEEE transactions on cybernetics*, 53(5): 2864–2875.

Jiang, Y.; Cao, Z.; and Zhang, J. 2021b. Solving 3D bin packing problem via multimodal deep reinforcement learning.

Khalil, E.; Dai, H.; Zhang, Y.; Dilkina, B.; and Song, L. 2017. Learning combinatorial optimization algorithms over graphs. *Advances in neural information processing systems*, 30.

Kocsis, L.; and Szepesvári, C. 2006. Bandit based monte-carlo planning. In *European conference on machine learning*, 282–293. Springer.

Laterre, A.; Fu, Y.; Jabri, M. K.; Cohen, A.-S.; Kas, D.; Hajjar, K.; Dahl, T. S.; Kerkeni, A.; and Beguir, K. 2018. Ranked reward: Enabling self-play reinforcement learning for combinatorial optimization. *arXiv preprint arXiv:1807.01672*.

Li, D.; Gu, Z.; Wang, Y.; Ren, C.; and Lau, F. C. 2022. One model packs thousands of items with recurrent conditional query learning. *Knowledge-Based Systems*, 235: 107683.

Li, D.; Ren, C.; Gu, Z.; Wang, Y.; and Lau, F. 2020. Solving packing problems by conditional query learning.

Li, Y.; Wang, S.; Sun, H.; and Zhou, S. 2025. Collaborative vessel–unmanned aerial vehicle routing for time-window-constrained offshore parcel delivery. *Transportation Research Part C: Emerging Technologies*, 178: 105189.

Li, Y.; Wang, S.; Zhou, S.; and Wang, Z. 2024. A mathematical formulation and a tabu search heuristic for the joint vessel-UAV routing problem. *Computers & Operations Research*, 169: 106723.

Liu, Z.; Meng, F.; Du, L.; Zhou, Z.; Yu, C.; Shao, W.; and Zhang, Q. 2025. CPGD: Toward Stable Rule-based Reinforcement Learning for Language Models. *arXiv preprint arXiv:2505.12504*.

Loshchilov, I.; and Hutter, F. 2017. Decoupled weight decay regularization. *arXiv preprint arXiv:1711.05101*.

Luo, F.; Lin, X.; Liu, F.; Zhang, Q.; and Wang, Z. 2023. Neural combinatorial optimization with heavy decoder: Toward large scale generalization. *Advances in Neural Information Processing Systems*, 36: 8845–8864.

Martello, S.; Pisinger, D.; and Vigo, D. 2000a. The three-dimensional bin packing problem. *Operations research*, 48(2): 256–267.

Martello, S.; Pisinger, D.; and Vigo, D. 2000b. The three-dimensional bin packing problem. *Operations research*, 48(2): 256–267.

Schrijver, A. 2002. Combinatorial Optimization: Theory and Algorithms.

Sutton, R. S. 1988. Learning to predict by the methods of temporal differences. *Machine learning*, 3(1): 9–44.

Veres, M.; and Moussa, M. 2019. Deep learning for intelligent transportation systems: A survey of emerging trends. *IEEE Transactions on Intelligent transportation systems*, 21(8): 3152–3168.

Wang, B.; Lin, Z.; Kong, W.; and Dong, H. 2025a. Bin packing optimization via deep reinforcement learning. *IEEE Robotics and Automation Letters*.

Wang, S.; Yu, L.; Gao, C.; Zheng, C.; Liu, S.; Lu, R.; Dang, K.; Chen, X.; Yang, J.; Zhang, Z.; et al. 2025b. Beyond the 80/20 rule: High-entropy minority tokens drive effective reinforcement learning for llm reasoning. *arXiv preprint arXiv:2506.01939*.

Wu, W.; Fan, C.; Huang, J.; Liu, Z.; and Yan, J. 2023. Machine learning for the multi-dimensional bin packing problem: Literature review and empirical evaluation. *arXiv preprint arXiv:2312.08103*.

Wu, X.; Wang, D.; Wen, L.; Xiao, Y.; Wu, C.; Wu, Y.; Yu, C.; Maskell, D. L.; and Zhou, Y. 2024. Neural combinatorial optimization algorithms for solving vehicle routing problems: A comprehensive survey with perspectives. *arXiv preprint arXiv:2406.00415*.

Wu, Y.; Li, W.; Goh, M.; and De Souza, R. 2010. Three-dimensional bin packing problem with variable bin height. *European journal of operational research*, 202(2): 347–355.

Xiong, H.; Guo, C.; Peng, J.; Ding, K.; Chen, W.; Qiu, X.; Bai, L.; and Xu, J. 2024. GOPT: Generalizable online 3D bin packing via transformer-based deep reinforcement learning. *IEEE Robotics and Automation Letters*.

Yang, S.; Song, S.; Chu, S.; Song, R.; Cheng, J.; Li, Y.; and Zhang, W. 2023. Heuristics integrated deep reinforcement learning for online 3d bin packing. *IEEE Transactions on Automation Science and Engineering*, 21(1): 939–950.

Zhang, J.; and Shuai, T. 2024. Online Three-Dimensional Bin Packing: A DRL Algorithm with the Buffer Zone. *Found. Comput. Decis. Sci.*, 49: 63–74.

Zhang, J.; Zi, B.; and Ge, X. 2021. Attend2pack: Bin packing through deep reinforcement learning with attention. *arXiv preprint arXiv:2107.04333*.

Zhao, A.; Li, T.; and Lin, L. 2024. A dynamic multi-modal deep reinforcement learning framework for 3D bin packing problem. *Knowledge-Based Systems*, 299: 111990.

Zhao, H.; She, Q.; Zhu, C.; Yang, Y.; and Xu, K. 2021. Online 3D bin packing with constrained deep reinforcement learning. In *Proceedings of the AAAI Conference on Artificial Intelligence*, volume 35, 741–749.

Zhao, H.; Yu, Y.; and Xu, K. 2021. Learning efficient online 3D bin packing on packing configuration trees. In *International conference on learning representations*.

Zhou, P.; Gao, Z.; Li, C.; and Chong, N. Y. 2024. An Efficient Deep Reinforcement Learning Model for Online 3D Bin Packing Combining Object Rearrangement and Stable Placement. In *2024 24th International Conference on Control, Automation and Systems (ICCAS)*, 964–969. IEEE.

## Appendix

In the section ‘‘Experiments: Generalization’’, we validate the performance of O4M-SP on various problem instances, including those with bin dimensions not encountered during training. In addition to MCTS (Kocsis and Szepesvári 2006), we also use a popular greedy algorithm employed by the major logistics firm we partner with as a baseline method. The greedy algorithm, illustrated in Algorithm 1, is based on the greedy algorithms proposed by Martello, Pisinger, and Vigo (2000b) and Crainic, Perboli, and Tadei (2008). In essence, the algorithm explores possible packing solutions through an ordered evaluation strategy, ensuring computational efficiency while maintaining effectiveness.

Algorithm 1: Greedy Algorithm for 3D-Bin Packing

---

**Input:** Bin dimensions  $(L, W, H)$ , item set  $I = \{I_1, \dots, I_n\}$  where  $I_j = (l_j, w_j, h_j)$   
**Output:** Loading rate  $\rho$

- 1: Initialize:  $V \leftarrow 0$ ,  $H_{\max} \leftarrow 0$ ,  $P \leftarrow \emptyset$ , corner set  $C \leftarrow \{(0, 0, 0)\}$
- 2: Sort items in  $I$  by volume in descending order (tie-breaking by longest side), resulting in  $I'$
- 3: **for** each item  $(l_j, w_j, h_j) \in I'$  **do**
- 4:     Sort corner set  $C$  by  $(z, y, x)$  in ascending order
- 5:      $placed \leftarrow \text{false}$
- 6:     **for** each corner  $(x, y, z) \in C$  **do**
- 7:         **for** each rotation  $(l, w, h)$  of item  $(l_j, w_j, h_j)$  **do**
- 8:             **if**  $x + l \leq L$  **and**  $y + w \leq W$  **and**  $z + h \leq H$  **then**
- 9:                  $overlap \leftarrow \text{false}$
- 10:                 **for** each placed item  $(x_p, y_p, z_p, l_p, w_p, h_p) \in P$  **do**
- 11:                     **if**  $(x < x_p + l_p)$  **and**  $(x + l > x_p)$  **and**  $(y < y_p + w_p)$  **and**  $(y + w > y_p)$  **and**  $(z < z_p + h_p)$  **and**  $(z + h > z_p)$  **then**
- 12:                          $overlap \leftarrow \text{true}$
- 13:                     **break**
- 14:             **end if**
- 15:         **end for**
- 16:         **if** **not**  $overlap$  **then**
- 17:              $P \leftarrow P \cup (x, y, z, l, w, h)$
- 18:              $V \leftarrow V + l \cdot w \cdot h$
- 19:              $H_{\max} \leftarrow \max(H_{\max}, z + h)$
- 20:              $C \leftarrow C \setminus (x, y, z) \cup \{(x + l, y, z), (x, y + w, z), (x, y, z + h)\}$
- 21:              $placed \leftarrow \text{true}$
- 22:             **break**
- 23:         **end if**
- 24:     **end if**
- 25:     **end for**
- 26:     **if**  $placed$  **then**
- 27:         **break**
- 28:     **end if**
- 29:     **end for**
- 30: **end for**
- 31:  $\rho \leftarrow \frac{V}{L \times W \times H_{\max}}$
- 32: **return**  $\rho$

---

Algorithm 1 aims to maximize the loading rate  $\rho$ . It takes the bin dimensions  $(L, W, H)$  and the item set  $I = \{I_1, \dots, I_n\}$  as input, where each item  $I_j$  is defined by its dimensions  $(l_j, w_j, h_j)$ . Step 1 sets the total volume of placed items  $V$  to 0, the maximum loading height  $H_{\max}$  to 0, initializes the set of placed items  $P$  as an empty set, and defines the initial corner set  $C = \{(0, 0, 0)\}$ . Step 2 sorts the item set  $I$  in descending order of volume, resulting in the ordered set  $I'$ . Steps 3-30 process each item in  $I'$  sequentially: the algorithm first sorts the available corner set  $C$  in ascending order by  $(z, y, x)$  coordinates to prioritize lower positions; then, it iterates over each corner  $(x, y, z) \in C$  and evaluates all possible rotations of the item. When an item, in a given rotation, satisfies the spatial constraints  $x + l \leq L$ ,  $y + w \leq W$ , and  $z + h \leq H$ , and does not overlap with any other item in the set  $P$ , it is placed into the bin. We update set  $P$ , the volume  $V$ , the maximum height  $H_{\max}$  and maintain the corner set  $C$  by updating it with new corner points  $(x + l, y, z)$ ,  $(x, y + w, z)$ , and  $(x, y, z + h)$ . Finally, in Step 31, the loading rate  $\rho$  is computed.